DOI: https://doi.org/10.1109/TIA.2024.3472647

This article has been accepted for publication in IEEE Transactions on Industry Applications. This is the author's version which has not been fully edited and content may change prior to final publication. Citation information: DOI 10.1109/TIA.2024.3472647

Fast Finite Element Based Vibration Response Calculation Procedure for Permanent Magnet Synchronous Machines

Mikel Mendizabal, Alex McCloskey, Sergio Zarate, Javier Poza and Gaizka Almandoz, *Member, IEEE*

***Abstract*—The vibration of the stator frame due to electromagnetic forces is one of the main noise and vibration sources of electric machines. In some applications, due to the wide variety of working conditions, magnetic circuit design optimisations are not enough, and the control of the machine is needed to reduce vibrations. Therefore, this work presents a reduced model, to be used during the control, which is able to estimate the stator frame vibrations of a Permanent Magnet Synchronous Machine. Finite Element calculations are performed, and the results are saved in Look-Up Tables and implemented in a calculation procedure, allowing a fast vibration estimation for any input conditions. The proposed model demonstrated the same accuracy as Finite Element simulations, with a calculation time of several seconds. The model was validated using experimental measurements, and it reliably estimated the evolution of the vibration of a commercial machine under varying current and rotational speed. Its potential to test harmonic current injection strategies was also experimentally corroborated. Thus, the model presented in this work is suitable to be further developed and implemented as a virtual sensor in a harmonic injection control procedure.**

***Index Terms*—Electric machines, Electromagnetic modeling, Finite Element analysis, Harmonic current injection, Metamodeling, Numerical simulation, Permanent magnet machines, Table lookup, Vibration measurement, Vibrations**

I. Introduction

PERMANENT Magnet Synchronous Machines (PMSM) are used in a wide variety of applications, due to their high torque density [1], [2]. In most applications, the comfort of the users is becoming a critical requirement, and thus, it is essential to optimise the vibration response of the machines. Among all the sources of noise and vibration, the vibrations of the stator frame generated by electromagnetic forces are among the most critical ones [2].

In literature, several approaches were presented to optimise the vibration response of PMSMs by design improvements [3], [4]. However, due to the wide operation range required in many applications, it is very complex to establish an optimum design for all working conditions, because excitation frequencies change with the rotational speed, and the amplitudes of the harmonics change with the loading conditions [5], [6]. Therefore, an alternative approach is to reduce the vibrations by means of control.

Most of the control strategies proposed in literature are based on modifying the current introduced to the machine, so that certain harmonics of the magnetic pressure, and consequently, certain harmonics of vibrations, are reduced. Harmonic current injection [5], [7] or current profile optimisation [6], [8] are some of the most employed techniques.

However, so that the control is effective for any working condition, the actual vibration state of the machine needs to be known. Some authors employ measurements provided by accelerometers as the input of the control [5], [9], [10], but that increases the cost and complexity of the control. In order to avoid the use of additional elements, a model to estimate the vibration of the machine can be used as a virtual sensor.

In order to obtain an accurate estimation of the vibrations of the stator, a multi-physical model needs to be developed. An electromagnetic model is needed to estimate the magnetic forces produced by electromagnetic phenomena, and a structural model is needed to estimate the dynamic response produced by those forces [11], [12].

The Finite Element Method (FEM) is a tool that is widely used to analyse various machine typologies. For instance, Finite Element (FE) models were developed for Induction Machines (IM) [13], [14], Switched Reluctance Machines (SRM) [15], [16], and PMSMs [1], [2], [17], [18], in order to estimate their vibration and noise response. Despite its high accuracy, the computational requirements of FEM are too high to be used in a dynamic control, where a calculation time below a few seconds might be required.

Analytical models offer faster calculations. In literature, analytical models were also employed for various machine typologies, such as IMs [19], [20], SRMs [21] and PMSMs [22]–[25]. Nevertheless, their accuracy is not high enough due to the simplifications and assumptions made to obtain the analytical solution. In order to develop an effective control, a calculation procedure that offers the accuracy of FEM is needed, with a computational effort low enough to be used in real time.

In [26] and [27], FE analyses were performed to estimate the electromagnetic torque for various current and rotor position values. The results were saved as Look Up Tables (LUT) and introduced to the models, avoiding FE calculations when the control is working.

In this work, a similar approach based on LUTs is proposed

This work was financially supported by the Basque Government under VEGAN KK21-004, EPOGAN KK-2023/00091 and Predoctoral Grant, and by the Provincial Council of Gipuzkoa under NVHCONTROL.

M. Mendizabal and A. McCloskey are with the Mechanical and Manufacturing Department, Mondragon Unibertsitatea, Mondragon, 20500, Spain (e-mail: mmendizabal@mondragon.edu, amccloskey@mondragon.edu).

S. Zarate, J. Poza and G. Almandoz are with the Electronics and Computing Department, Mondragon Unibertsitatea, Mondragon, 20500, Spain (e-mail: szarate@mondragon.edu, jpoza@mondragon.edu, galmandoz@mondragon.edu).

to fulfil the mentioned requirements. Complex FE models were created and simulations were performed in a wide range of conditions. The results of the simulations were gathered in LUTs and implemented in the model, creating a fast and simple tool that provides the output result for any input parameters.

This calculation procedure was presented in [28], where it showed the accuracy of the FE models with a substantial reduction of calculation time. In this extended paper, the experimental validation of the model is added to the FE validation in [28]. The performance of the proposed model is tested at various working conditions.

As previously mentioned, the model is conceived to be implemented in a control strategy, with the objective of reducing the vibration response of an electric machine in its entire range of working conditions. A harmonic current injection technique could be employed, where the model developed in this work would work as a virtual sensor, and based on the vibration estimation it provided, the control would introduce a specific current harmonic to reduce the most problematic vibration harmonic.

For that purpose, the model needs to reliably predict the vibration response of the machine under varying working conditions. The main objective of the model is not a high accuracy in amplitudes, but predicting the evolution of the vibration harmonics when varying the rotational speed and load of the machine. As it will be part of a real-time control, the prediction of the model needs to be fast enough. A calculation time about 100 times slower than real time would be reasonable to validate control strategies. In order to use the model in the control, the calculation time should be close to real time.

In Section II, the calculation procedure is described. A detailed explanation of the electromagnetic and structural models is given. In Section III, the calculation procedure is validated employing both FE simulations and experimental measurements. In Section IV, the main conclusions of the paper are summarised.

II. Model of the Machine

The PMSM analysed in this work is a machine employed for elevation systems. Its main characteristics are summarised in Table I. In this application, there are rather strict regulations regarding the maximum allowable vibration level of the electric machines, as the vibration and noise that is transmitted to the environment is amplified through the structures the machines are mounted in.

TABLE I: Machine Characteristics.

Number of slots	36
Number of pole pairs	15
Number of winding layers	2
Rated power	7 kW (9 HP)
Rated rotational speed	300 rpm

According to the ISO 20816 standard [29], a limit of around 1 mm/s (*rms*) is established for low-power machine vibrations. Generally, the vibration level of the PMSM analysed in this work is below that limit, but there is a significant variability among different machine units and buildings they are mounted in. In addition, the standard is focused on total vibration energy, but certain machine units show specific vibration harmonics with excessive amplitude, which is also harmful.

The model of the machine was developed in the Matlab/Simulink simulation platform [30]. Fig. 1 shows an overview of the workflow of the model. The inputs are the rotational speed of the machine (ω) and the current in *dq* axes (I_d and I_q). First, with the electromagnetic model, the electromagnetic pressure ($\mathbf{q}$) on the stator teeth surface is obtained. Then, the pressure is used as the input of the structural model to calculate the vibration ($\ddot{\mathbf{u}}$) at the surface of the stator frame.

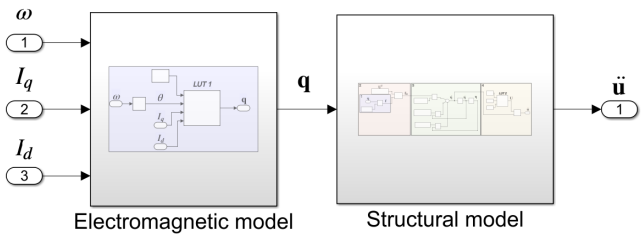

Fig. 1: Overview of the developed reduced model.

A. Electromagnetic Model

The electromagnetic model is a surrogate model, which consists in a LUT that relates the rotor position and the current introduced to the machine with the magnetic pressure on the stator teeth. The radial (q_r) and tangential (q_t) components of the pressure are obtained using Maxwell's tensor [31]:

$$q_r = \frac{B_r^2 - B_t^2}{2\mu_0} \qquad q_t = \frac{B_r B_t}{\mu_0} \tag{1}$$

where B_r and B_t are the radial and tangential components of the magnetic flux density and μ_0 is the magnetic permeability of the air.

It is assumed that the vibrations of the frame mainly occur due to the radial component of the pressure, and that the tangential component does not have a considerable impact [31]. Thus, in order to simplify the model and reduce the computational cost, only the radial pressure was considered in the calculation procedure.

In order to build the LUT, the magnetic flux density on the surface of the teeth needs to be known, for any rotor position and current value. For that purpose, a FE model of the machine was created using FLUX software [32], following the procedure explained in [33]. Using that model, a simulation sweep was defined, consisting of the following current values:

- I_d: [-3; -2; -1; -0.8; -0.6; -0.4; -0.2; 0; 0.2; 0.4; 0.6; 0.8; 1; 2; 3] A (*rms*).
- I_q: [-13.3; -9; -6.5; -4; -2; -1.5; -1; -0.8; -0.6; -0.4; -0.2; 0; 0.2; 0,4; 0.6; 0.8; 1; 1.5; 2; 4; 6.5; 9; 13.3] A (*rms*).

A total of 345 simulations were performed, each of them using one of the previous I_d and I_q values as inputs. Then,

the magnetic flux density obtained in all the simulations was gathered to build the electromagnetic LUT.

As the machine analysed in this work has a non-skewed rotor, the pressure is constant along the axial direction of the stator. Thus, a 2D FE model was defined.

Assuming the machine ideal, it is not necessary to perform the simulations for the entire geometry. To reduce the computational cost, just one winding periodicity was considered, which corresponds to the third part of the machine, and the results were then repeated three times to complete the entire machine.

As it is a magnetostatic calculation, each time increment refers to a certain angular position of the rotor (θ). The resolution of the rotor position is defined by the maximum temporal electric order ($r_{\max}$) that can be correctly analysed without aliasing. Thus, the number of rotor positions (N_θ) can be defined according to:

$$N_\theta = r_{\max} p k \tag{2}$$

where p is the number of pole pairs and k the number of points per period needed to correctly define each frequency order. In accordance with (2), in order to represent the 30$^{\text{th}}$ temporal electric order and considering 6 points per period, 2700 rotor positions would be needed in the entire machine. But being an ideal machine, it is not necessary to simulate an entire mechanical period, one electrical period is enough. Thus, 180 rotor positions were defined.

In order to obtain the spatial distribution of the pressure for every rotor position, a path was defined along the stator teeth. The number of points per tooth (N_{t}) defines the maximum spatial electric order ($s_{\max}$) that can be correctly estimated without aliasing:

$$N_{\text{t}} = \frac{\alpha_{\text{t}} s_{\max} p k}{2\pi} \tag{3}$$

where α_{t} is the angle of a tooth. According to (3), in order to represent the 30$^{\text{th}}$ spatial electric order, and considering 6 points per period, 40 points per tooth were defined.

In each simulation, the radial and tangential components of the magnetic flux density (B_r and B_t) were exported, for all the points defined in the path, for each rotor position.

The data was gathered in the matrices $\mathbf{B}_r(I_d, I_q, \theta, \alpha)$ and $\mathbf{B}_t(I_d, I_q, \theta, \alpha)$, where θ is the rotor position and α is the spatial angular position. Then, applying Maxwell's tensor, the radial pressure matrix $\mathbf{q}_r(I_d, I_q, \theta, \alpha)$ was obtained and implemented as LUT 1 in the electromagnetic model (Fig. 2).

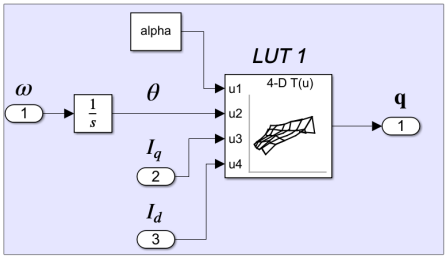

Fig. 2: Overview of the developed electromagnetic model.

B. Structural Model

Starting from the pressure on the surface of the teeth obtained by the electromagnetic model, the structural model was defined to calculate the vibration of the stator frame.

The calculation procedure was developed in accordance with the equation of the motion of the mechanical system [34]:

$$\mathbf{M}\ddot{\mathbf{u}} + \mathbf{C}\dot{\mathbf{u}} + \mathbf{K}\mathbf{u} = \mathbf{f} \tag{4}$$

where $\mathbf{M}$, $\mathbf{C}$ and $\mathbf{K}$ are the mass, damping and stiffness matrices, $\mathbf{u}$ is the displacement vector and $\mathbf{f}$ the force vector.

Solving the previous equation in the matrix form is very time consuming. However, the equation system can be decoupled applying the modal superposition method [34], which considers that the motion is the sum of the contribution of the vibration modes of the system. In accordance with this method, the response of the system is the product of the mode shape matrix ($\mathbf{U}$) and the modal amplitude vector ($\boldsymbol{\eta}$):

$$\mathbf{u} = \mathbf{U}\boldsymbol{\eta} \tag{5}$$

If the transpose of the mode shape matrix is pre-multiplied to all the elements, the equation of the motion is written as:

$$\mathbf{U}^{\text{T}}\mathbf{M}\mathbf{U}\ddot{\boldsymbol{\eta}} + \mathbf{U}^{\text{T}}\mathbf{C}\mathbf{U}\dot{\boldsymbol{\eta}} + \mathbf{U}^{\text{T}}\mathbf{K}\mathbf{U}\boldsymbol{\eta} = \mathbf{U}^{\text{T}}\mathbf{f} \tag{6}$$

Assuming that the damping of the system can be modelled with modal damping, equation (6) can be rewritten using the modal mass, modal damping and modal stiffness matrices:

$$\mathbf{M}_{\text{D}}\ddot{\boldsymbol{\eta}} + \mathbf{C}_{\text{D}}\dot{\boldsymbol{\eta}} + \mathbf{K}_{\text{D}}\boldsymbol{\eta} = \mathbf{f}_{\text{D}} \tag{7}$$

where $\mathbf{M}_{\text{D}}$, $\mathbf{C}_{\text{D}}$ and $\mathbf{K}_{\text{D}}$ are diagonal matrices, being all the non-diagonal elements equal to zero. The k-th elements of the diagonals (m_k, c_k, k_k), correspond to the modal mass, modal damping and modal stiffness of mode k.

Therefore, the equation system is decoupled, and a set of differential equations, equal to the number of modes considered in the analysis, is obtained:

$$m_k\ddot{\eta}_k + c_k\dot{\eta}_k + k_k\eta_k = f_k \tag{8}$$

By dividing all the terms by the modal mass, and knowing that $c_k = 2\xi_k\omega_k m_k$ and $k_k = \omega_k^2 m_k$, the equation is rewritten as:

$$\ddot{\eta}_k + 2\xi_k\omega_k\dot{\eta}_k + \omega_k^2\eta_k = f_k/m_k \tag{9}$$

where ξ_k and ω_k are the damping ratio and the natural frequency of mode k, and f_k is the effective force on mode k.

The effective force is the scalar product of the modal shape of a mode and the spatial distribution of the force vector, as shown in equation (10). The closer the spatial distribution of the force is to the shape of a mode, the higher the contribution of that mode to the vibration will be.

$$f_k = U_k\mathbf{f} \tag{10}$$

This article has been accepted for publication in IEEE Transactions on Industry Applications. This is the author's version which has not been fully edited and content may change prior to final publication. Citation information: DOI 10.1109/TIA.2024.3472647

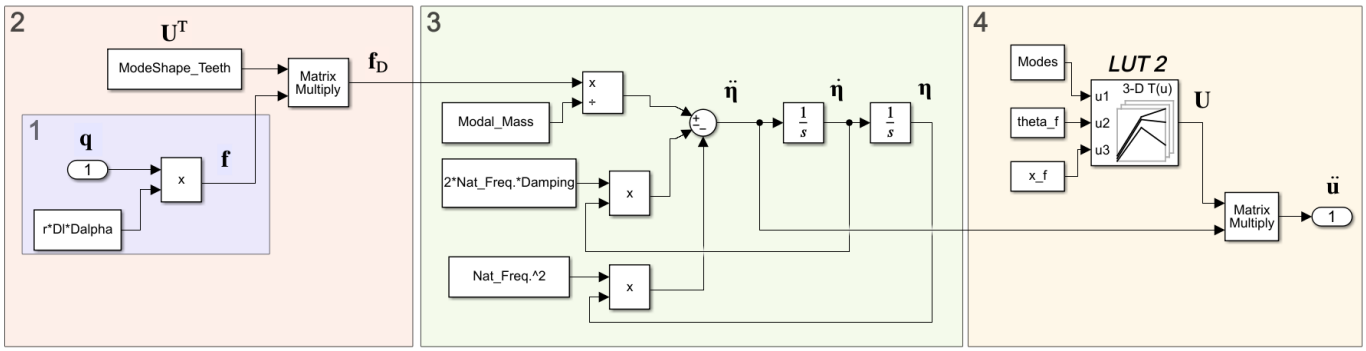

Fig. 3: Overview of the developed structural model.

The differential equation is solved for each mode and the modal amplitude vector is obtained. Equation (5) is used to obtain the vibration response of the system. Multiplying the mode shape matrix with the modal amplitude vector, the displacement at any point of the machine is obtained.

Fig. 3 shows the structural model developed in this work, which is divided in four steps. The model was defined in accordance with the calculation procedure explained in the previous paragraphs, and in order to calculate the mode shape matrices that are necessary for the calculations, a FE model of the machine was created using ABAQUS software [35]. The FE model was defined as explained in [36].

Step 1) Calculation of the Force Vector: The pressure obtained from the electromagnetic model is used as the input of the structural model. The pressure is converted into the force vector $\mathbf{f}$, by considering the area that corresponds to each of the points of the structural mesh:

$$\mathbf{f} = \mathbf{q}_r R \Delta L \Delta \alpha \tag{11}$$

where R is the inner radius of the stator, and ΔL and $\Delta \alpha$ are the axial and angular dimensions of the mesh.

Step 2) Calculation of the Effective Force Vector: Using the FE model, the vibration modes of the system are calculated, in order to obtain the mode shape matrix that is needed to calculate the effective force vector $\mathbf{f}_{\mathrm{D}}$.

When the modal superposition method is used, it is convenient to calculate the modes in a higher range than the frequency range of interest for the response, as higher frequency modes may also have a considerable impact on lower frequencies. In this work, the upper limit for the response is the 30$^{\text{th}}$ electric order. A typical reference is to consider twice the frequency range of the response, but in order to ensure that no relevant modes are neglected, it was decided to calculate all the modes within 5 times the frequency range of the response.

The vibration modes contain the movement of every single point of the model, but in order to develop (10) and calculate the effective force vector, the mode shape only on the stator teeth surface, which is the area where the force is applied, is required.

As mentioned in Section II-A, the number of points per tooth defines the maximum spatial order that can be correctly estimated without aliasing. According to (3), 40 points per tooth were also defined for the structural FE model, in order to reach the 30$^{\text{th}}$ spatial electric order.

The pressure is constant along the axial direction of the stator, but the machine is not axially symmetrical, and the modal shapes vary in that direction. Therefore, 5 axial sections were defined in the stator, and for each axial position, a path was defined along the edge of the stator teeth. Then, for every mode, a vector containing the motion of all the points in each path was exported. Only the radial component of the motion was exported, as the tangential component of the pressure was neglected.

Step 3) Resolution of the Differential Equation: Equation (9) is solved, and the modal amplitude vector $\boldsymbol{\eta}$ is obtained. The modal mass vector, which is divided to the effective force, was also exported from the FE calculation.

Step 4) Calculation of the Vibration on the Stator Frame: Finally, the vibration on the external surface of the stator is calculated using (5). In this step, the mode shape matrix on the outer surface of the stator is required, which was also exported from the FE calculation.

The results were gathered in the LUT 2 of Fig. 3, which contains the mode shape matrix for any tangential (θ_{f}) and axial (x_{f}) position of the surface. Multiplying the values of the mode shapes at the point of interest with the modal amplitude vector, and summing the results obtained for all the modes, the vibration of that specific point of the stator frame is obtained.

III. Validation of the Model

First, the accuracy and the response time of the model proposed in this work was compared to FE calculations, in order to validate its performance compared to the conventional FE calculation procedure. Then, the prediction of the model was validated using experimental results, in order to ensure that it provides a realistic estimation of the behaviour of the machine under various working conditions.

A. Finite Element Simulations

The first part of the validation was performed by comparing the vibration response obtained in FE simulations to the response estimated by the proposed reduced model running in Simulink. The central point of the upper face of the stator frame was chosen as the reference point, as shown in Fig. 4.

This article has been accepted for publication in IEEE Transactions on Industry Applications. This is the author's version which has not been fully edited and content may change prior to final publication. Citation information: DOI 10.1109/TIA.2024.3472647

Fig. 4: Reference point in the structural FE model.

The rated working point of the machine was selected for the comparison, consisting in a rotational speed of 300 rpm and an I_q current of 9 A (*rms*). The response until 0.5 s was calculated, with a time increment of 5 µs, both in the FE simulations and the reduced model.

The FE simulation consisted in a coupling between FLUX and ABAQUS. First, the selected current and rotational speed were introduced to FLUX, and a magnetostatic calculation was performed. The spatial distribution of the pressure on the teeth was exported for every time increment. Then, the pressure was introduced to ABAQUS, and a modal dynamic calculation was performed, in order to obtain the vibration response of the machine. The same spatial mesh was used in both FE models, in order to minimise errors when transferring the pressure.

As the current is constant over time, once the transient response is attenuated, a steady-state response is obtained.

Fig. 5 shows the vibration velocity spectrum in the transient region. The estimation of the general trend and the peak frequencies is highly accurate, except for several low-frequency amplitudes that are underestimated by the reduced model.

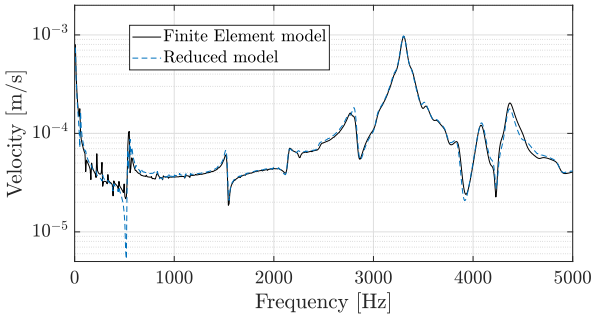

Fig. 5: Comparison of the reduced model prediction and FE simulations in the transient region.

Fig. 6 shows the vibration velocity spectrum in the steady-state region. The amplitude of the frequency components is estimated very accurately. The most significant differences are observed at high-order harmonics.

Those differences in amplitudes might be due to an error made in the transition between the two FE software, when applying the electromagnetic pressure into the structural FE software. The structural FE software converts the pressure on the stator teeth surface into forces, distributing it in all the nodes defined in the mesh of the surface. Depending on the size of the elements, some information may be lost.

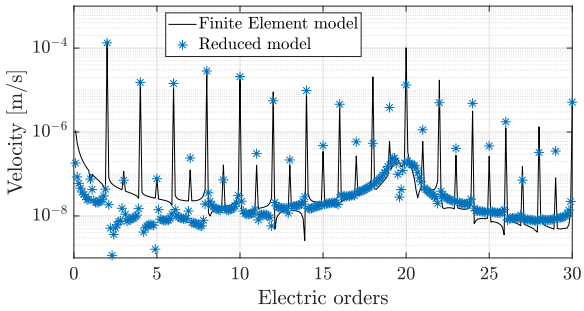

Fig. 6: Comparison of the reduced model prediction and FE simulations in the steady-state region.

The electromagnetic FE model has 75000 elements and 160000 nodes, and the simulation required a computational time of 12 hours in a 12 core and 96 GB RAM computer. The structural model has 2500000 elements and 3100000 nodes, and the simulation required 36 hours. In contrast, the calculation was performed in 50 seconds by the reduced model in Simulink.

B. Experimental Measurements

The reduced model shows highly accurate results compared to FE calculations, but it is necessary to validate if its prediction is close to the experimental behaviour of real machines. For that purpose, two mass-produced commercial machines (two units of the same model, hereinafter referred to as M1 and M2) were tested in operation under various working conditions. The main characteristics of the tested machine model are shown in Table I.

1) Experimental Set-Up: The set-up for the experimental measurements is shown in Fig. 7. The machine under test was fixed on a test bench and coupled to a secondary machine that was used to apply the necessary load. An accelerometer was placed on the machine, in order to measure the vibration on the center of the upper surface. The current of the three-phases and the rotational speed of the rotor were also measured.

Fig. 7: Set-up for the experimental measurements.

The following equipment was used for the measurements:

- Acquisition system Pulse Brüel & Kjær Front-end type 3560C and a laptop with Pulse Labshop software.
- ICP triaxial accelerometer of PCB 356A16. Frequency range: From 0.5 Hz to 5000 Hz. Sensitivity: 100 mV/g.
- Three Fluke i310s AC/DC current clamps.
- Rotational transducer (encoder).

This article has been accepted for publication in IEEE Transactions on Industry Applications. This is the author's version which has not been fully edited and content may change prior to final publication. Citation information: DOI 10.1109/TIA.2024.3472647

To be a reliable control strategy, the model needs to be valid for various working conditions. The following tests were performed, to check if the model is able to estimate the evolution of the vibration response with respect to the working conditions:

- Constant speed measurements at no load.
- Constant speed measurements at variable load.
- Variable speed measurements at no load.
- Harmonic current injection tests.

In order to replicate the same working conditions corresponding to the experimental tests, the current and the rotational speed signals of each test were used as the inputs of the model.

2) Constant Speed Measurements at No Load: In this test, the machines were rotating at 150 rpm, which is half of their rated speed, at no load. The vibration response was measured during 30 seconds, which corresponds to 75 revolutions. With this, the average of the spectrum was obtained in order to reduce the experimental variability.

The instantaneous values of the current and the rotational speed signals were introduced to the model, and the resulting vibration was calculated for every time increment. The calculation was carried out for two revolutions. As the calculation is in time-domain, a transient response is obtained, and thus, a long enough time needs to be simulated in order to reach the steady-state condition response, which is the working condition that is analysed in this section.

The rotational speed of the machine and the current in *dq* axes should be constant during the tests, but some variations will occur in reality, which might affect the estimation of the model. Thus, the influence of using the experimental input signals, in comparison to ideal constant values, was analysed. The signals corresponding to machine M1 were selected.

Fig. 8 shows that the amplitude of the main integer vibration harmonics remains almost unchanged regardless of the input definition. The only effect of considering the experimental signals as inputs is that noise between even harmonics is obtained.

Thus, it is demonstrated that the current and rotational speed ripples generate a nearly-uniform noise between the integer harmonics, without producing notable additional harmonics. When considering the experimental signals as the inputs, the model is able to predict the experimental noise with a high accuracy regarding the amplitude, making the estimation of the model very similar to the measured vibration level.

However, the main frequency components of the vibration are the integer harmonics. Those are the only frequency components that an ideal machine will have, and thus, they are generally the predominant harmonics. Thus, for control purposes, the rotational speed and current reference values assigned by the control would be enough to predict the behaviour of the machine, without the need of measuring the actual instantaneous values.

Therefore, the comparison between the experimental and estimated vibration spectra at constant speed can be performed using Fig. 8b. The general trend of the integer harmonics is predicted well by the reduced model. The most significant differences are observed in electric orders 6 and 12, which

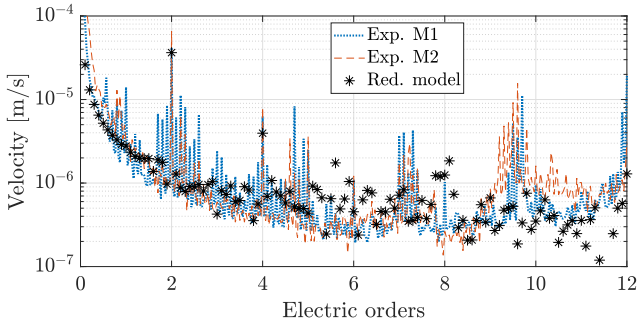

(a) Experimental current and rotational speed

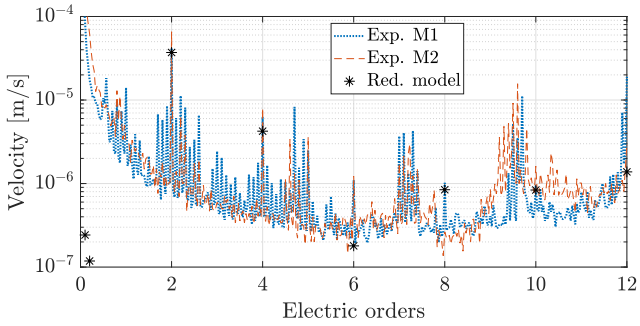

(b) Constant current and rotational speed

Fig. 8: Vibration spectra at 150 rpm employing different input definitions.

are underestimated with respect to the experimental results. However, the amplitudes of electric orders 2, 4, 8 and 10 are close to the experimental values.

In the experimental results, there are several fractional harmonics (around 2.4, 4.8, 7.2 or 9.6) with significant amplitudes, which are not predicted by the reduced model. These fractional harmonics are produced by the imperfections or tolerances of the commercial machines.

Every part has dimensional tolerances; when manufacturing a machine, the real dimensions of its components will deviate in some extent from the ideal values. Thus, all machines will have a certain amount of eccentricity and imperfections in the rotor and stator, which will modify the shape of the magnetic flux in the air gap, producing additional harmonics of the pressure at any mechanical order [37]–[39]. In particular, the tolerances of the permanent magnets and the rotor produce vibration harmonics at mechanical orders multiple to the number of stator slots [37], which correspond to electric orders multiple to 2.4 for the analysed PMSM.

The model in this work was defined for an ideal machine, and thus, it cannot show any effect of the imperfections or manufacturing tolerances of the machine. Therefore, all the harmonics that arise due to tolerances are not predicted by the model, and that is why those harmonics cannot be compared. If fractional harmonics were harmful or significant for the machine or application of interest, the FE model would need to be developed considering manufacturing tolerances.

It is also worth mentioning that there is certain variability between the two machine units. The general trend is very similar in both cases, but there are notable differences at some

This article has been accepted for publication in IEEE Transactions on Industry Applications. This is the author's version which has not been fully edited and content may change prior to final publication. Citation information: DOI 10.1109/TIA.2024.3472647

harmonics, mainly at the fractional ones, due to the particular imperfections of each machine unit.

3) Constant Speed Measurements at Variable Load: In this case, the machines were also rotating at 150 rpm, but a different load level was introduced in each test. For each load case, the vibration was measured during 30 seconds in order to obtain the steady-state response.

From these tests, the evolution of the even integer vibration harmonics (up to electric order 12) with respect to the load was studied. As mentioned previously, the amplitudes of several harmonics were not accurately predicted by the reduced model, but its main purpose is to correctly estimate the evolution of the harmonics, rather than their precise amplitudes. For that reason, the relative variation of the harmonic amplitudes, taking the zero-load value as a reference, was studied in this section, as shown in Fig. 9.

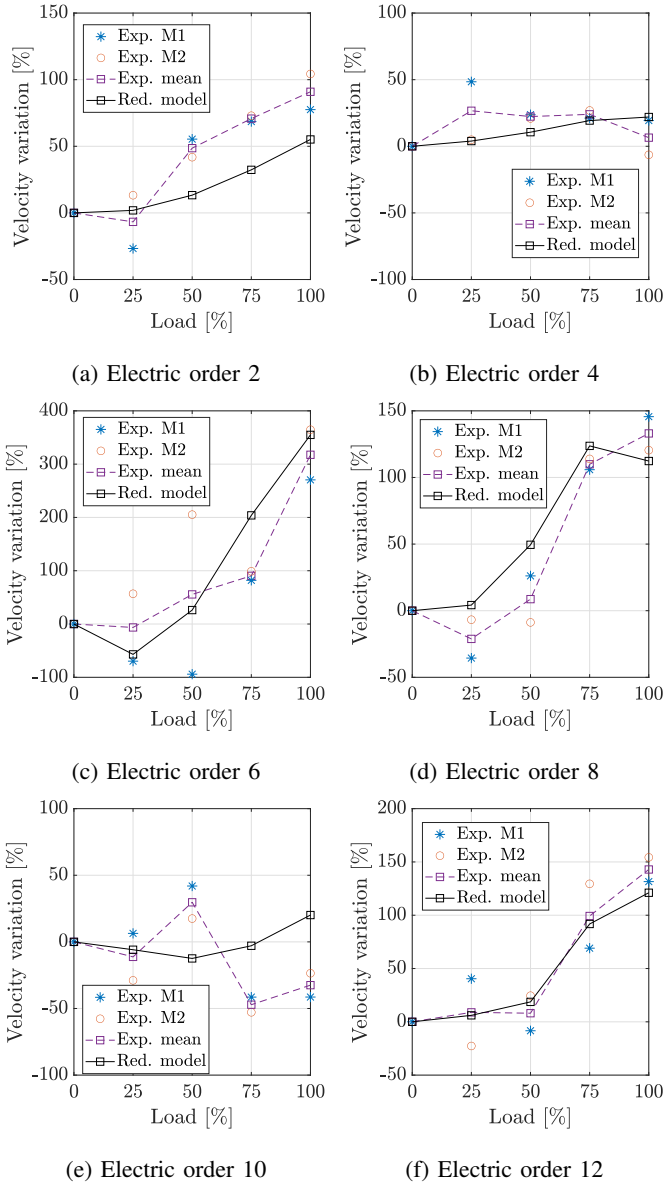

(a) Electric order 2 (b) Electric order 4

(c) Electric order 6 (d) Electric order 8

(e) Electric order 10 (f) Electric order 12

Fig. 9: Evolution of each vibration harmonic over load.

Certain variability is observed between the two tested machines. As mentioned previously, the particular imperfections of each machine have a considerable effect on the vibration harmonics. However, the evolution of the harmonics with respect to the load is similar in the two cases, and comparing the mean value of both tests to the prediction of the model, it can be said that the trend of all harmonics is well estimated by the model.

In Fig. 10, the evolution of all the even integer harmonics is compared. Both in the model and experimentally, electric order 6 is the most sensitive harmonic to load, followed by orders 8 and 12. Electric order 2 also shows an increasing trend, slightly underestimated by the model. Finally, orders 4 and 10 seem to be independent respect to the load, as they do not show a clear trend neither experimentally nor in the model.

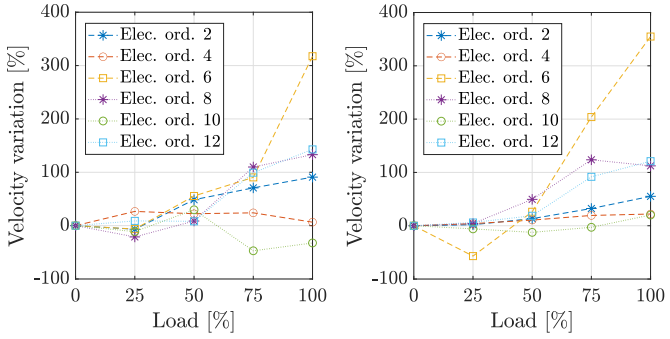

(a) Experimental (mean value) (b) Reduced model

Fig. 10: Evolution of vibration harmonics over load.

4) Variable Speed Measurements at No Load: In this test, a run-up or velocity sweep was performed at no load, varying the rotational speed of the motors from 0 to 300 rpm (rated speed). The vibration response was measured during the test, and the evolution of the main vibration harmonics in function of the rotational speed was obtained.

The velocity sweep was reproduced in the reduced model, by introducing the experimental rotational speed of every time increment as an input. That way, the dynamic behaviour of the machine was estimated employing a single simulation. In Fig. 11 and Fig. 12, the evolution of electric orders 2 and 4 is shown.

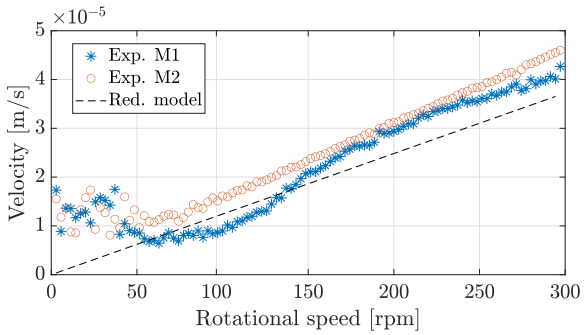

Fig. 11: Evolution of electric order 2 of vibration over rotational speed.

This article has been accepted for publication in IEEE Transactions on Industry Applications. This is the author's version which has not been fully edited and content may change prior to final publication. Citation information: DOI 10.1109/TIA.2024.3472647

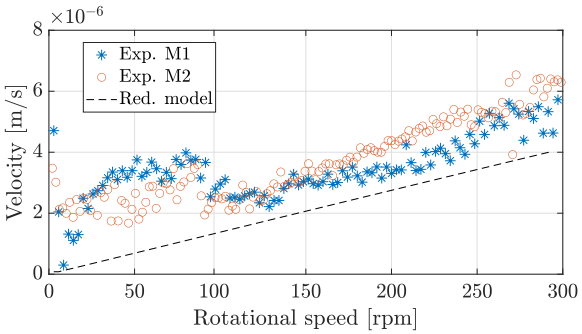

Fig. 12: Evolution of electric order 4 of vibration over rotational speed.

For both harmonics, the experimental trend is unclear at low rotational speeds. Due to the low vibration level at low speeds, the harmonics can be hardly distinguished from the background noise. Moreover, at low rotational speeds, the control of the machine introduces higher currents to obtain the torque needed to keep the reference speed. At low speed, the momentum is low, and the effect of friction is bigger; and thus, it is harder to keep the velocity at the desired value. As it can be seen in Fig. 13, higher I_q harmonics are introduced at low speed, which produce higher vibration values. Thus, the experimental data below 100 rpm is considered unreliable.

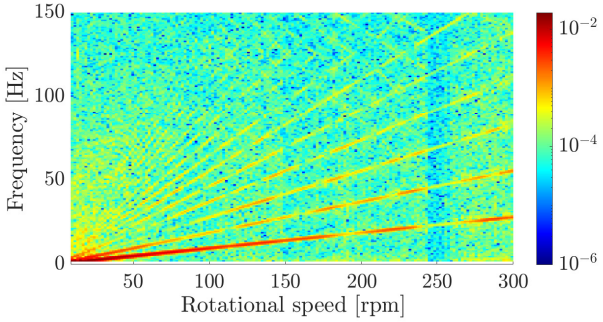

Fig. 13: Spectrogram of I_q.

At higher rotational speeds the experimental trend of both harmonics is accurately estimated by the reduced model. A linear relationship between the harmonic amplitude and the rotational speed is obtained, as expected, because electric orders 2 and 4 do not reach any natural frequency in the rotational speed range covered.

In Fig. 14, the evolution of electric order 20 as a function of rotational speed is shown. In this case, a resonance is clearly observed in the experimental results at around 250 rpm. The same phenomenon is predicted by the model. Even though there is a small error on the natural frequency (≈15-20 rpm), the model is able to predict the significant amplification of electric order 20 when the excitation frequency is close to a natural frequency of the machine.

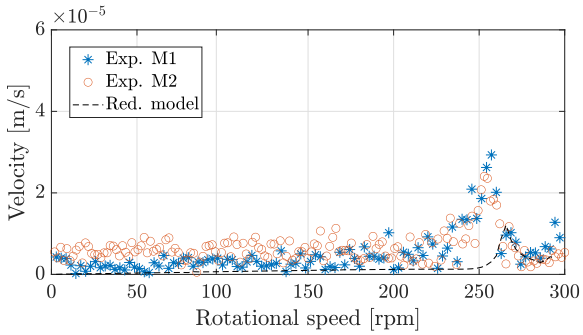

Fig. 14: Evolution of electric order 20 of vibration over rotational speed.

5) Harmonic Current Injection Tests: Having validated the performance of the model under varying working conditions, its potential to be used in a harmonic injection control procedure is analysed in this section.

The harmonic injection technique consists in injecting harmonics in the current to reduce a certain problematic vibration harmonic. In order to obtain the reduction of the vibration harmonic of interest, the optimum amplitude and phase of the harmonic of the current need to be deduced.

In accordance with the spectra analysed in Fig. 8, electric orders 2 and 4 are the most significant vibration harmonics of the machine (both experimentally and in the model). Thus, two harmonic injection strategies were defined:

- Injection of the 2^{nd} electric order of I_d, with the objective of reducing the 2^{nd} electric order of the vibration.
- Injection of the 4^{th} electric order of I_d, with the objective of reducing the 4^{th} electric order of the vibration.

In both cases, a constant speed of 150 rpm at no load was set as the test conditions.

In order to find the optimum amplitude and phase of the current harmonics that would result in the greatest vibration reduction, an optimisation process was carried out using the reduced model. Simulation sweeps were performed, varying the amplitude and the phase of the injected current harmonic between 0-3 A and 0-360°, respectively. Fig. 15 shows the amplitude of the vibration harmonic respect to the amplitude and phase of the corresponding current harmonic.

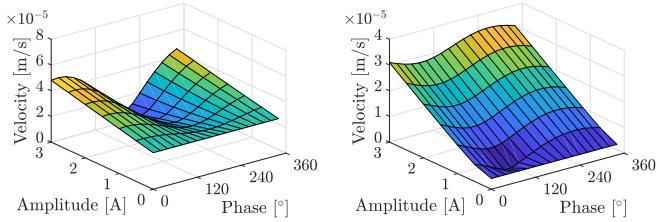

(a) Electric order 2 (b) Electric order 4

Fig. 15: Vibration amplitude with respect to the amplitude and phase of the same I_d harmonic.

According to the optimisation process, both vibration harmonics can be potentially reduced. The optimum values for the amplitude and phase of the current harmonics are gathered in Table II.

This article has been accepted for publication in IEEE Transactions on Industry Applications. This is the author's version which has not been fully edited and content may change prior to final publication. Citation information: DOI 10.1109/TIA.2024.3472647

TABLE II: Optimum amplitude and phase of the I_d harmonics.

I_d Harmonic	Amplitude	Phase
2	3 A	200°
4	0.5 A	100°

Experimental measurements were performed to validate if the current harmonics proposed by the model are effective in reducing the desired vibration harmonics. For that purpose, two new constant speed tests (at 150 rpm and no load) were performed with the machine M1, in each test injecting one of the optimised current harmonics deduced by the model.

Apart from the harmonic to be reduced, it is also interesting to analyse how the rest of the vibration harmonics are modified when injecting the current. For that reason, the variation of all the even vibration harmonics (up to electric order 12) was analysed, taking the original (no harmonic injection) vibration spectrum as a reference.

Fig. 16 shows the variation of the vibration harmonics when injecting the 2$^{\text{nd}}$ electric order of I_d. A significant reduction of electric order 2 of vibration is experimentally achieved, as desired, and the reduction is similar to the one predicted by the model (87% versus 92%). However, the current injection produces higher amplitudes in other vibration harmonics. A particularly significant alteration of electric order 4 is observed experimentally, with a similar increase as the one predicted by the model (270% versus 308%). The model also predicts increments of orders 8, 10 and 12. Only electric order 8 is increased experimentally as estimated, as order 10 is reduced and order 12 remains almost unchanged. However, in these electric orders, neither the alterations predicted by the model nor the experimental ones have a significant impact on the general response.

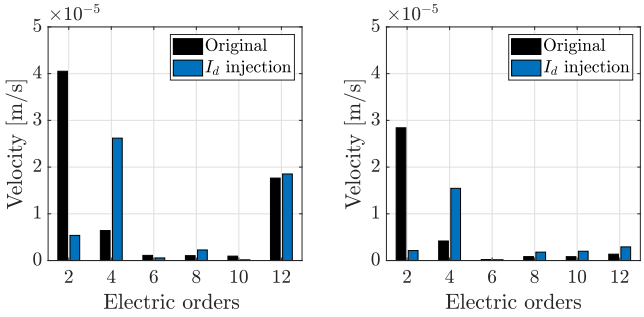

(a) Experimental (b) Reduced model

Fig. 16: Evolution of vibration harmonics when injecting electric order 2 of I_d.

Fig. 17 shows the variation of the vibration harmonics when injecting the 4$^{\text{th}}$ electric order of I_d. A notable reduction of the desired vibration harmonic (electric order 4) is also achieved experimentally, the reduction being similar to the one predicted by the model (78% versus 59%). In this case, the rest of the harmonics do not undergo significant variations, neither experimentally nor in the model.

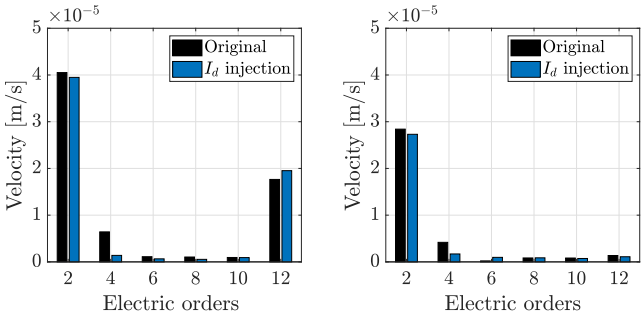

(a) Experimental (b) Reduced model

Fig. 17: Evolution of vibration harmonics when injecting electric order 4 of I_d.

Overall, the potential of the model to test control strategies was experimentally corroborated, as the current harmonics defined by the model proved to effectively reduce the addressed vibration harmonics. However, it was also observed that other vibration harmonics may be altered due to the current injection. As the model also predicts this phenomenon, it can be employed to test new injection strategies to optimise the global behaviour of the machine.

IV. Conclusions

This work presents a reduced model to estimate the vibration response of the stator frame of PMSMs. An electromagnetic model and a structural model were created, both based on LUTs that gather the information obtained in complex and time-consuming FE simulations.

The proposed model reduces the calculation time of conventional FE calculations from a significant amount of hours to a few seconds, without compromising the accuracy of the results. The performance of the model was also validated experimentally, in comparison to mass-produced commercial machines.

The results show that the model is able to predict the evolution of the main vibration harmonics with respect to the load and rotational speed of the machine. The main differences between the prediction obtained with the model and the experimental measurements were observed at fractional harmonics that arise due to imperfections derived from manufacturing tolerances and eccentricities. However, these differences were expected, since the model developed was defined considering the machine ideal. If the machine is considered ideal the LUT of the electromagnetic model can be obtained with a much lower computation time, but the complete real behaviour of the machine is not obtained. Therefore, if the fractional harmonics are significant or need to be reduced by the control, the model should consider manufacturing tolerances in order to predict the harmonics due to imperfections accurately.

The short calculation time of the model makes it suitable to be employed for the validation of control strategies. Harmonic current injection tests were performed, and the potential of the model to test control strategies was corroborated. The model was employed to estimate the optimum amplitude and phase of the current harmonics to be injected, and by injecting those

harmonics, a significant reduction of the addressed vibration harmonics was achieved experimentally.

The reduced model also predicted an undesired increase of other vibration harmonics when injecting certain current harmonics, which was also observed in the experimental measurements. Even if a specific harmonic is cancelled, the global vibration behaviour of the machine might be worsened. Thanks to the model proposed it is possible to calculate the harmonics that need to be introduced in order to reduce the desired harmonic without worsening the global vibration response. These quick calculations can be performed within an optimisation procedure to find the optimum current to be injected.

Finally, with further reduction of the calculation time, by optimizing the electromagnetic LUT, the number of modes and the integration algorithm, the model could be suitable to be employed as a virtual sensor in a harmonic current injection control strategy.

REFERENCES

[1] K. Qian, J. Wang, Y. Gao, Q. Sun, and J. Liang, "Interior noise and vibration prediction of permanent magnet synchronous motor," *Journal of Vibroengineering*, vol. 20, no. 5, pp. 2225–2236, 2018.

[2] D. Torregrossa, F. Peyraut, B. Fahimi, J. Mboua, and A. Miraoui, "Multiphysics finite-element modeling for vibration and acoustic analysis of permanent magnet synchronous machine," *IEEE Transactions on Energy Conversion*, vol. 26, no. 2, pp. 490–500, 2011.

[3] C. Gan, J. Wu, Q. Sun, W. Kong, H. Li, and Y. Hu, "A review on machine topologies and control techniques for low-noise switched reluctance motors in electric vehicle applications," *IEEE Access*, vol. 6, pp. 31 430–31 443, 2018.

[4] S. H. Lee, J. P. Hong, S. M. Hwang, W. T. Lee, J. Y. Lee, and Y. K. Kim, "Optimal Design for Noise Reduction in Interior Permanent-Magnet Motor," *IEEE Transactions on Industry Applications*, vol. 45, no. 6, pp. 1954–1960, 2009.

[5] L. Kang, J. Xia, H. Su, Z. Li, and S. Liu, "On-line control strategy for radial vibration suppression of PMSM by multi-harmonic current injection method," *IEEE Transactions on Industrial Electronics*, pp. 1–1, 2021.

[6] M. Kawa, K. Kiyota, J. Furqani, and A. Chiba, "Acoustic noise reduction of a high-efficiency switched reluctance motor for hybrid electric vehicles with novel current waveform," *IEEE Transactions on Industry Applications*, vol. 55, no. 3, pp. 2519–2528, 2019.

[7] S. Jiang and Y. Wang, "Tangential Force Noise Reduction of Vehicular PMSM Based on Reference Harmonic Current Analytical Computation," *IEEE Transactions on Transportation Electrification*, vol. 9, no. 2, pp. 2081–2089, 2023.

[8] A. D. Callegaro, B. Bilgin, and A. Emadi, "Radial Force Shaping for Acoustic Noise Reduction in Switched Reluctance Machines," *IEEE Transactions on Power Electronics*, vol. 34, no. 10, pp. 9866–9878, 2019.

[9] A. J. den Hamer, G. Z. Angelis, and N. B. Roozen, "Broad-band active vibration suppression using PPF focused on industrial application," *IEEE/ASME Transactions on Mechatronics*, vol. 10, no. 2, pp. 146–153, 2005.

[10] X. Ojeda, X. Mininger, H. B. Ahmed, M. Gabsi, and M. Lécrivain, "Piezoelectric actuator design and placement for switched reluctance motors active damping," *IEEE Transactions on Energy Conversion*, vol. 24, no. 2, pp. 305–313, 2009.

[11] J. Le Besnerais, "Fast prediction of variable-speed acoustic noise due to magnetic forces in electrical machines," in *2016 XXII International Conference on Electrical Machines (ICEM)*, Lausanne, Switzerland, 2016, pp. 2259–2265.

[12] H. Fang, D. Li, R. Qu, and P. Yan, "Modulation effect of slotted structure on vibration response in electrical machines," *IEEE Transactions on Industrial Electronics*, vol. 66, no. 4, pp. 2998–3007, 2019.

[13] S. Sathyan, U. Aydin, and A. Belahcen, "Acoustic noise computation of electrical motors using the boundary element method," *Energies*, vol. 13, no. 1, p. 245, 2020.

[14] V. Climente-Alarcon, A. Arkkio, and J. Antonino-Daviu, "2-D Magnetomechanical Transient Study of a Motor Suffering a Bar Breakage," *IEEE Transactions on Industry Applications*, vol. 54, no. 3, pp. 2097–2104, 2018.

[15] J. Furqani, C. A. Wiguna, A. Chiba, O. Gundogmus, Y. Sozer, and A. Purwadi, "Experimental Verification of Acoustic Noise and Radial Force Sum Variation in Switched Reluctance Motor," *IEEE Transactions on Industry Applications*, vol. 57, no. 3, pp. 2481–2493, 2021.

[16] F. L. Dos Santos, J. Anthonis, F. Naclerio, J. J. Gyselinck, H. Van Der Auweraer, and L. C. Góes, "Multiphysics NVH modeling: Simulation of a switched reluctance motor for an electric vehicle," *IEEE Transactions on Industrial Electronics*, vol. 61, no. 1, pp. 469–476, 2014.

[17] M. S. Islam, R. Islam, and T. Sebastian, "Noise and vibration characteristics of permanent-magnet synchronous motors using electromagnetic and structural analyses," *IEEE Transactions on Industry Applications*, vol. 50, no. 5, pp. 3214–3222, 2014.

[18] M. Valavi, A. Nysveen, R. Nilssen, and T. Rolvag, "Slot harmonic effect on magnetic forces and vibration in low-speed permanent-magnet machine with concentrated windings," *IEEE Transactions on Industry Applications*, vol. 50, no. 5, pp. 3304–3313, 2014.

[19] J. Le Besnerais, V. Lanfranchi, M. Hecquet, P. Brochet, and G. Friedrich, "Prediction of audible magnetic noise radiated by adjustable-speed drive induction machines," *IEEE Transactions on Industry Applications*, vol. 46, no. 4, pp. 1367–1373, 2010.

[20] G. Bauw, F. Balavoine, B. Cassoret, O. Ninet, and R. Romary, "Equivalent Circuit of PWM-Fed Induction Machine with Damper Winding for Noise and Vibration Reduction," *IEEE Transactions on Industry Applications*, vol. 54, no. 5, pp. 4147–4155, 2018.

[21] J. O. Fiedler, K. A. Kasper, and R. W. De Doncker, "Calculation of the acoustic noise spectrum of SRM using modal superposition," *IEEE Transactions on Industrial Electronics*, vol. 57, no. 9, pp. 2939–2945, 2010.

[22] M. Mendizabal, A. McCloskey, J. Poza, S. Zarate, J. Iriondo, and L. Irazu, "Optimum slot and pole design for vibration reduction in permanent magnet synchronous motors," *Applied Sciences (Switzerland)*, vol. 11, no. 11, p. 4849, 2021.

[23] A. McCloskey, X. Arrasate, X. Hernández, I. Gómez, and G. Almandoz, "Analytical calculation of vibrations of electromagnetic origin in electrical machines," *Mechanical Systems and Signal Processing*, vol. 98, pp. 557–569, 2018.

[24] R. Islam and I. Husain, "Analytical model for predicting noise and vibration in permanent-magnet synchronous motors," *IEEE Transactions on Industry Applications*, vol. 46, no. 6, pp. 2346–2354, 2010.

[25] Z. Q. Zhu, Z. P. Xia, L. J. Wu, and G. W. Jewell, "Analytical modeling and finite-element computation of radial vibration force in fractional-slot permanent-magnet brushless machines," *IEEE Transactions on Industry Applications*, vol. 46, no. 5, pp. 1908–1918, 2010.

[26] Y. Kano, K. Watanabe, T. Kosaka, and N. Matsui, "A novel approach for circuit-field-coupled time-stepping electromagnetic analysis of saturated interior PM motors," *IEEE Transactions on Industry Applications*, vol. 45, no. 4, pp. 1325–1333, 2009.

[27] X. Chen, J. Wang, B. Sen, P. Lazari, and T. Sun, "A high-fidelity and computationally efficient model for interior permanent-magnet machines considering the magnetic saturation, spatial harmonics, and iron loss effect," *IEEE Transactions on Industrial Electronics*, vol. 62, no. 7, pp. 4044–4055, 2015.

[28] M. Mendizabal, A. McCloskey, S. Zarate, and J. Poza, "Fast and accurate vibration response calculation procedure for permanent magnet synchronous machines," in *2022 International Conference on Electrical Machines (ICEM)*, Valencia, Spain, 2022, pp. 2207–2213.

[29] International Organization for Standardization, "Mechanical vibration - Measurement and evaluation of machine vibration." ISO Standard No. 20816-3:2022, 2022.

[30] The MathWorks Inc., "MATLAB version: 9.12.0 (R2022a)," Natick, Massachusetts, United States, 2022.

[31] P. Pennacchi, "Computational model for calculating the dynamical behaviour of generators caused by unbalanced magnetic pull and experimental validation," *Journal of Sound and Vibration*, vol. 312, no. 1-2, pp. 332–353, 2008.

[32] Altair, "Altair Flux 2021.2.0," Troy, Michigan, United States, 2021.

[33] S. Zarate, A. Egea, G. Almandoz, A. Mccloskey, U. Galfarsoro, and A. Urdangarin, "A study of the effects of the magnetization tolerance in the manufacturing process on permanent magnet synchronous machines," in *2020 10th International Electric Drives Production Conference, EDPC*, Ludwigsburg, Germany, 2020, pp. 1–8.

[34] S. S. Rao, *Mechanical Vibrations*, 3rd ed., Addison-Wesley Longman, Ed., New York, 1995.

[35] Dassault Systèmes Simulia Corp., "ABAQUS/CAE 6.14," Paris, France, 2014.
[36] A. McCloskey, X. Arrasate, X. Hernandez, and O. Salgado, "Measurement and simulation of the vibroacoustic performance of an electric motor," *Mechanisms and Machine Science*, vol. 23, pp. 339–348, 2015.
[37] U. Galfarsoro, A. McCloskey, S. Zarate, X. Hernández, and G. Almandoz, "Influence of Manufacturing Tolerances and Eccentricities on the Unbalanced Magnetic Pull in Permanent Magnet Synchronous Motors," *IEEE Transactions on Industry Applications*, vol. 58, no. 3, pp. 3497–3510, 2022.
[38] G. Bramerdorfer, "Tolerance Analysis for Electric Machine Design Optimization: Classification, Modeling and Evaluation, and Example," *IEEE Transactions on Magnetics*, vol. 55, pp. 1–9, 2019. [Online]. Available: https://api.semanticscholar.org/CorpusID:198146599
[39] B. M. Ebrahimi, M. Javan Roshtkhari, J. Faiz, and S. V. Khatami, "Advanced Eccentricity Fault Recognition in Permanent Magnet Synchronous Motors Using Stator Current Signature Analysis," *IEEE Transactions on Industrial Electronics*, vol. 61, no. 4, pp. 2041–2052, 2014.

Alex McCloskey was born in Dublin, Ireland. He received the B.Sc. and M.Sc. degrees in Mechanical Engineering and Industrial Engineering from Mondragon Unibertsitatea in 2009 and 2012 respectively. He developed his Ph.D. thesis about vibrations of electrical machines in Mondragon Unibertsitatea.

Since 2016, he has been with the Acoustics and Vibrations Group of the Mechanics and Manufacturing department of the Faculty of Engineering of Mondragon Unibertsitatea, where he is currently a Lecturer and Researcher. His current research interests include electrical machines design and diagnosis. He has participated in a number of research projects in the fields of elevator drives and railway traction.

Sergio Zarate was born in Vitoria-Gasteiz, Spain. He received the B.Sc., M.Sc. and Ph.D. degrees in Electrical Engineering from Mondragon Unibertsitatea, Mondragon, Spain, in 2012, 2014 and 2018, respectively.

Since 2018, he has been with the Electronics department of the Faculty of Engineering of Mondragon Unibertsitatea, where he is currently a Lecturer and Researcher. His current research interests include drives, electrical machines vibration and permanent magnet machine design and optimisation.

Mikel Mendizabal was born in Zumaia, Spain. He received the B.Sc. and M.Sc. degrees in Mechanical Engineering and Industrial Engineering from Mondragon Unibertsitatea in 2019 and 2021 respectively.

Since 2021, he has been with the Electronics department of the Faculty of Engineering of Mondragon Unibertsitatea, where he is currently a Ph.D. Student. His current research interests include electrical machines vibration modelling and control.

Javier Poza was born in Bergara, Spain, in June 1975. He received the B.S. degree in Electrical Engineering from Mondragon Unibertsitatea, in 1999 and the Ph.D. degree in electrical engineering from the Institut National Polytechnique de Grenoble, Grenoble, France.

Since 2002, he has been with the Electronics department of the Faculty of Engineering of Mondragon Unibertsitatea, where he is currently an Associate Professor. His current research interests include electrical machine design, modelling, diagnostic and control. He has participated in various research projects in the fields of electric vehicles, wind energy systems, lift drives, and railway traction.

Gaizka Almandoz (M'04) was born in Arantza, Spain, in March 1979. He received the B.S. and Ph.D. degrees in electrical engineering from Mondragon Unibertsitatea, Mondragon, Spain, in 2003 and 2008, respectively.

Since 2003, he has been with the Department of Electronics, Faculty of Engineering, Mondragon Unibertsitatea, where he is currently an Associate Professor. His current research interests include electrical machine design, modeling, and control. He has participated in various research projects in the fields of renewable energy and people transportation systems.